Molecular mixing in Rayleigh–Taylor instability. Part I: Global mixing

P. F. Linden and J. M. Redondo
Department of Applied Mathematics and Theoretical Physics, University of Cambridge, Silver Street, Cambridge CB3 9EW, England

(Received 10 September 1990; accepted 25 January 1991)

This paper describes experiments on the mixing produced by Rayleigh–Taylor instability between two miscible fluids. A layer of brine is placed over a layer of fresh water in a gravitational field, and the ensuing flow is visualized by laser-induced fluorescence and measurements are made of the concentration fields as the flow develops. It is found that large-scale disturbances develop which produce intermingling of the fluids, but molecular mixing occurs as a result of small-scale instabilities which grow on the edges of the larger scale motions. When the system overturns stably stratified fluid is produced, and the mixing efficiency of the process is measured and found to be large compared with other forms of mixing. It is suggested that this increased efficiency is due to the fact that much of the mixing occurs when the system is unstably stratified.

I. INTRODUCTION

Rayleigh–Taylor (RT) instability occurs at an interface between dense fluid and less dense fluid when the latter is at a higher pressure. The most familiar example is that of heavy fluid lying on top of light fluid in a gravitational field. Another example is the case of laser-induced implosion of glass encapsulated deuterium targets. These targets are spherical and, during the implosion process, high pressures develop in the less dense deuterium as the glass shell decelerates and RT instability ensues.

In many practical circumstances it is important to determine the amount of mixing that occurs between the fluids as a result of the RT instability. An important component of the overall mixing in stratified fluids is due to overturning processes, such as breaking internal waves or Kelvin–Helmholtz billows, in which local density inversions are produced. For atmospheric and oceanic flows estimates of the vertical mixing are required in order to parametrize these mixing processes in numerical models.

In this paper we present an investigation on the mixing produced by a turbulent, unstably stratified flow. The aim of the research is to determine the amount of molecular mixing that occurs during the RT instability process using laboratory experiments. The modeling approach adopted here is to use two miscible liquids, with the dense liquid accelerated by gravity toward the less dense liquid. The properties of the mixing process are examined using a range of laboratory techniques as outlined below.

The stability of an interface between two superposed fluids of different density was studied by Rayleigh,[1] and Taylor[2] carried out a linear stability analysis and noted that the conditions for instability may occur in acceleration fields other than gravity. A good summary of the linear theory can be found in Chandrasekhar.[3] For inviscid fluids the interface is always unstable, with the growth rate of the unstable modes increasing as their wavelengths decrease. The instability of the short waves can be reduced by surface tension or viscosity, and then linear theory predicts the maximum growth rate to occur at a finite wavelength. For the viscous two-layer case, where the upper layer (density ρ_1) is denser than the lower layer (density ρ_2), the wavelength λ_m of maximum growth rate is

$$\lambda_m \approx 4\pi[\nu^2(\rho_1+\rho_2)/g(\rho_1-\rho_2)]^{1/3}, \tag{1}$$

where ν is the mean kinematic viscosity of the two layers and g is the acceleration of gravity. The corresponding maximum growth rate is

$$n_m \approx [g\pi(\rho_1-\rho_2)/\lambda_m(\rho_1+\rho_2)]^{1/2}. \tag{2}$$

While the linear theory for two infinite layers is well established, the development of the instability to finite amplitude is not amenable to analytic treatment. There have been a number of semianalytical and numerical studies in recent years, but they all involve simplifying assumptions which raise serious doubts about their validity, particularly when applications to mixing are sought.

A discussion of the subject by Youngs[4] characterized the development of the instability through three stages before breaking up into chaotic turbulent mixing. Initially, a perturbation of wavelength λ_m grows exponentially with growth rate n_m. When this perturbation reaches a height of approximately $\frac{1}{2}\lambda_m$, the growth rate decreases and larger structures appear. In the final stage the scale of dominant structures continues to increase and memory of the initial conditions is lost; viscosity does not appear to affect the growth of the large structures.

This latter result concerning the independence of the large amplitude structures on the initial conditions leads to the result that the width of the mixing region, which develops between the two layers, depends only on ρ_1, ρ_2, g, and time t. Then dimensional analysis gives

$$\delta = 2cg[(\rho_1-\rho_2)/(\rho_1+\rho_2)]t^2, \tag{3}$$

where c is a constant whose value may depend on the density ratio. It is convenient then to use this result to determine a time scale for the flow given by

$$T = (H/gA)^{1/2}, \tag{4}$$

where $A = (\rho_1-\rho_2)/(\rho_1+\rho_2)$ is the Atwood number and H is the depth of the fluid. This time scale gives a measure of the time it takes for the mixing region to extend throughout the fluid. The classic experiments on the evolution of a Ray-

 0899-8213/91/051269-09$02.00

leigh–Taylor front are those of Lewis[5] and Allred and Blount,[6] using an air–water interface. Many other experiments have been carried out since on different aspects of RT instability, most of them at high Atwood number (see Duff *et al.*;[7] Emmons *et al.*[8]). Most of these experiments have concentrated on the form and wavelengths of the unstable modes. Of particular note here are the experiments of Read[9] and Youngs[10] who measured the width of the mixing region with both immiscible and miscible fluids. For values of the Atwood number $A = 0.5$–1.0 they confirmed (3), and found values of c to be independent of ρ_1/ρ_2 in the range 0.030–0.035. Here we extend these earlier experimental studies by investigating the mixing processes that occur during the growth of RT instability to finite amplitude. The present paper concentrates on the growth of the mixing layer and the global properties of the mixing, including measurements of concentration fluctuations. Subsequent papers will discuss the detailed structure of the mixing interface.

The format of this paper is as follows. The present laboratory setup and the various techniques that are used are described in Sec. II. The results of the various techniques used to estimate the mixing process are presented in Sec. III, together with some measurements of the detailed mixing process at the interface. The discussion and conclusions are given in Sec. V.

II. EXPERIMENTS

A. Tank and experiment description

The present experiments were carried out in a Perspex tank 500 mm deep, 400 mm long, and 200 mm wide. The tank has a removable aluminum sheet 1.5 mm in thickness separating a layer of brine, density ρ_1, from a layer of fresh water, density ρ_2, below (see Linden *et al.*[11]). The two layers of fluid were initially at rest, and the experiment was initiated by sliding the aluminum sheet horizontally through a slit in one end wall of the tank. Routine flow visualization was either by shadowgraph or by adding dye to one of the layers. Records of the flow were made using video and still photography.

The experiments were conducted with two layers of equal depth, with a range of Atwood numbers $(\rho_1 - \rho_2)/(\rho_1 + \rho_2)$ from 1×10^{-4} to 5×10^{-2}. These values were chosen to enable sufficiently high Reynolds numbers to be achieved during the development of the instability, while ensuring there was sufficient time before the whole two-layer system overturned.

Quantitative measurements were made using the following techniques.

B. Conductivity measurements

A ten-channel conductivity meter, monitoring up to ten independent probes, was used to obtain measurements of salt concentration. The output of the conductivity meter was stored on a BBC computer via a CUBAN data processing system. Maximum sampling frequencies were 50 Hz, which corresponds to the fastest time response of the conductivity probes. A series of tests showed that the spatial response of the probes was approximately 1 mm (Redondo[12]).

The output of the conductivity probes was calibrated against the salt concentration (and temperature) of the solutions. The response was found to be linear over the range of density differences used, and accurate to 1% of the full scale reading. The dependence on temperature was minimized by carrying out all experiments at room temperature, having let the solutions stand overnight.

The conductivity probes were arranged in two different configurations. One set of experiments were carried out with a conductivity probe in the center of the tank, 1 mm above the separating plate. Density oscillations were measured as the RT front advanced and as the whole fluid overturned. In another set of experiments a single probe was mounted on a vertical traversing mechanism that spanned 400 mm. The density profiles were taken every 30 sec after the plate had been released, until no further change in the profiles was observed. Comparison between the initial and final profiles enabled the change in potential energy of the stratification as a result of the RT instability to be calculated (see Sec. IV).

C. Dye visualization

Small amounts of dye (food coloring) were added to one of the layers and the flow was observed as the instability progressed. Two main results were obtained from an analysis of these images.

(i) The maximum extent, 2δ, of the region of interpenetration of the two layers. This was measured directly from the video images. Anomalous regions were observed near the sides of the tank, and the values quoted below were taken from the central region.

(ii) Dye concentration. The values were obtained by determining the intensity of the light transmitted through the tank, using an image processing system on the digitized video frames. The dye concentration values are integrated across the width of the tank.

In order to resolve the detailed structure of the mixing region, the flow was also visualized by using a thin sheet of laser light to illuminate a plane perpendicular to the camera. Side, end, and plan views were obtained. A 2 W argon laser was used to produce a 2 mm thick sheet of high intensity light. Fluorescein dye was added to one of the layers, and this produced a brilliant green image in the laser light. The edge of the mixing region was clearly demarcated by this technique and images of the small-scale structures were obtained. Fractal analysis of the edge of the mixing region as well as a detailed study of the structure of the RT front was carried out, and will be presented in Redondo and Linden.[13] As with the dye measurements, the fluorescein is only added in very small quantities so that the dye acts as a passive tracer. The video images were analyzed using an automatic image processing system developed at DAMTP.

III. EXPERIMENTAL RESULTS

A. Qualitative observations

The ideal situation, with which the experiments are designed to correspond, is the instantaneous removal of the aluminum plate between the layers with no disturbance to the planar interface. In practice, however, vortices were shed from the trailing edge of the plate giving a large length scale

perturbation to the interface. In addition, the finite time required to remove the plate caused some asymmetry in the growth of the mixing layer. Observations also revealed anomalous regions near the side walls of the tank, where the growth of the mixing region is accelerated due to the presence of image vortices. All the quantitative measurements discussed below were made near the center of the tank where these edge effects are minimized. A detailed discussion of the quantitative effects of the plate removal are given in Redondo and Linden.[14]

The instability is characterized by the formation of small length scale disturbances. These disturbances are consistent with the linear modes given by (1) (see Linden *et al.*[11]). At later times the scale of the dominant instability increases usually as a result of pairing of the smaller scale structures. Further small-scale disturbances are generated, either by secondary RT instability, or by Kelvin–Helmholtz (KH) instability. The latter were typically observed to develop in regions of high shear along the sides of the larger-scale motions.

In experiments where plan view laser-induced fluorescence (LIF) was used to investigate the horizontal structure of the RT instability, three-dimensional blobs could be seen to grow despite the fact that the initial perturbations produced by the withdrawal of the plate were two dimensional. This observation provides additional confirmation that the effects of the plate removal do not persist, and that the growth of the mixing region and the nature of the observed disturbances appear to be independent of the initial conditions.

Superimposed on these wave motions are smaller-scale motions characteristic of mixing in stratified fluids. These eventually decay in the manner described by Pearson and Linden.[15]

B. Quantitative results

1. The thickness of the mixing region

Measurements of the half-width δ of the mixing region were taken from the flow visualization experiments. Both shadowgraphs, in which both edges of the mixing region were visible, and dye visualizations, in which only one edge was visible were used, and measurements were restricted to the central portion of the tank where the region was fairly uniform. The values of δ then correspond to averages over the horizontal area of the interface.

An example for one experiment is shown in Fig. 1. In accordance with (3) the data exhibit a quadratic time dependence on time t. A least-squares fit to the data with $(\delta/H)^{1/2}$ plotted against t/T is shown, and from this we see that the line does not pass through the origin. The mixing region has a finite initial thickness δ_0 that corresponds to the disturbances generated by the removal of the plate. In the example shown in Fig. 1, $\delta_0 = 0.8$ cm, which is consistent with the observed size of the vortices shed by the plate. This distance is small compared with the depth of the tank, and so may be neglected during the later growth of the mixing region, as suggested by the qualitative observations described above. Once the initial conditions are forgotten, the rate of growth

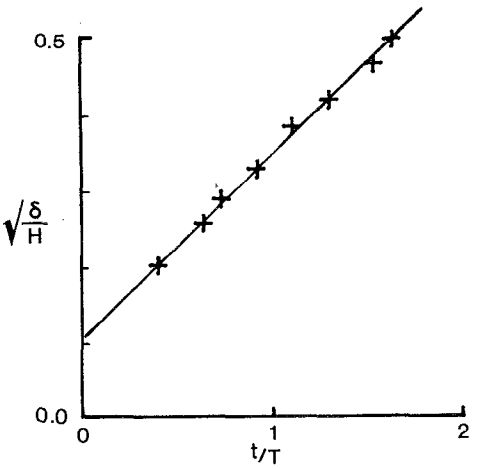

FIG. 1. Plot of the dimensionless mixing layer thickness $(\delta/H)^{1/2}$ against the nondimensional time t/T; δ_0 is the extrapolated value at $t = 0$.

of the mixing region depends only on δ, A, and g (assuming molecular effects are negligible). Dimensional analysis then gives

$$\frac{d\delta}{dt} = 2(2cgA\delta)^{1/2}, \tag{5}$$

and integration gives

$$\delta^{1/2} = \delta_0^{1/2} + (2cgAt^2)^{1/2}, \tag{6}$$

where the initial condition $\delta = \delta_0$ at $t = 0$ has been used. When the mixing region is thick $\delta \gg \delta_0$, (6) becomes $\delta = 2cgAt^2$, which recovers (3).

Values of c are determined from the slopes of plots such as shown in Fig. 1. A total of 49 experiments were carried out and the values of c are plotted against the Atwood number A in Fig. 2. At low values of A, the values of c are somewhat scattered due to the effects of the plate removal, but at higher values of A, c is approximately constant and takes the value

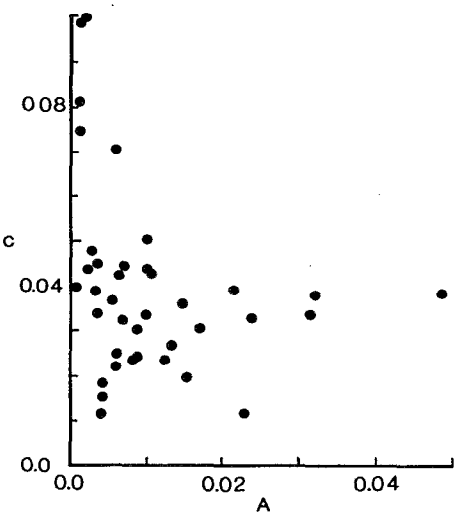

FIG. 2. Plot of c as a function of the Atwood number A.

$c = 0.035 \pm 0.005$. This value is in agreement with the values obtained at large density ratios ($0.5 < A < 1$) by Read[9] and Youngs,[10] and this agreement gives confidence that the present experiments are accurately modeling these earlier experiments.

2. Dense fluid volume fraction

Measurements of dye intensity were made which allow estimates of the dense fluid volume fraction to be made. Dye was added to the upper layer (concentration 1) while the lower layer was free of dye (concentration 0). By measuring the light intensity, and referring it to a calibrated sample, it is possible to determine the amount of dye along any horizontal line across the tank as a function of time. Assuming that the dye acts as a passive tracer, this measurement gives a width average of the fraction of dense fluid at any point as a function of time.

Video images of the experiment were digitized providing 513×513 pixel frames in up to 256 intensity levels. Nonuniformities in background lighting were removed by subtracting the initial background from each frame. Some care was necessary with this procedure to avoid TV line phase changes.

Examples of light intensity contours at different times obtained from an experiment with $A = 0.0015$ are shown in Fig. 3. The main feature to note from the figure is the relatively rapid change in light intensity at the edge of the descending dense fluid. The thickness of the transition region is about 1 cm, and this suggests that much of the mixing is occurring at the edges of the large-scale protuberances. Within the larger-scale structures the variations in concentration are relatively weak.

Vertical profiles of light intensity are shown in Figs. 4 and 5. These profiles show only the lower half of the tank, and are normalized so that initially the upper layer corresponds to unit concentration and lower layer to zero concentration. The dye intensities are also averaged across the central portion of the tank (i.e., away from the anomalous edge regions) in Fig. 4, so that the profiles represent averages over the horizontal area of the tank. The advance of the mixing region is clearly shown, with an approximately linear increase in mean dye concentration with height across the mixing region. From Fig. 3, and from the flow visualization studies, we know that the dense fluid falls as semicoherent large-scale structures. Figure 5 shows the vertical profiles through one of these structures, rather than averaged along the length of the tank as in Fig. 4. The rapid increase in dense fluid across the base of the structure, and the relatively uniform interior is clearly visible. We also note from Fig. 5 that the change in concentration becomes sharper as the disturbance advances.

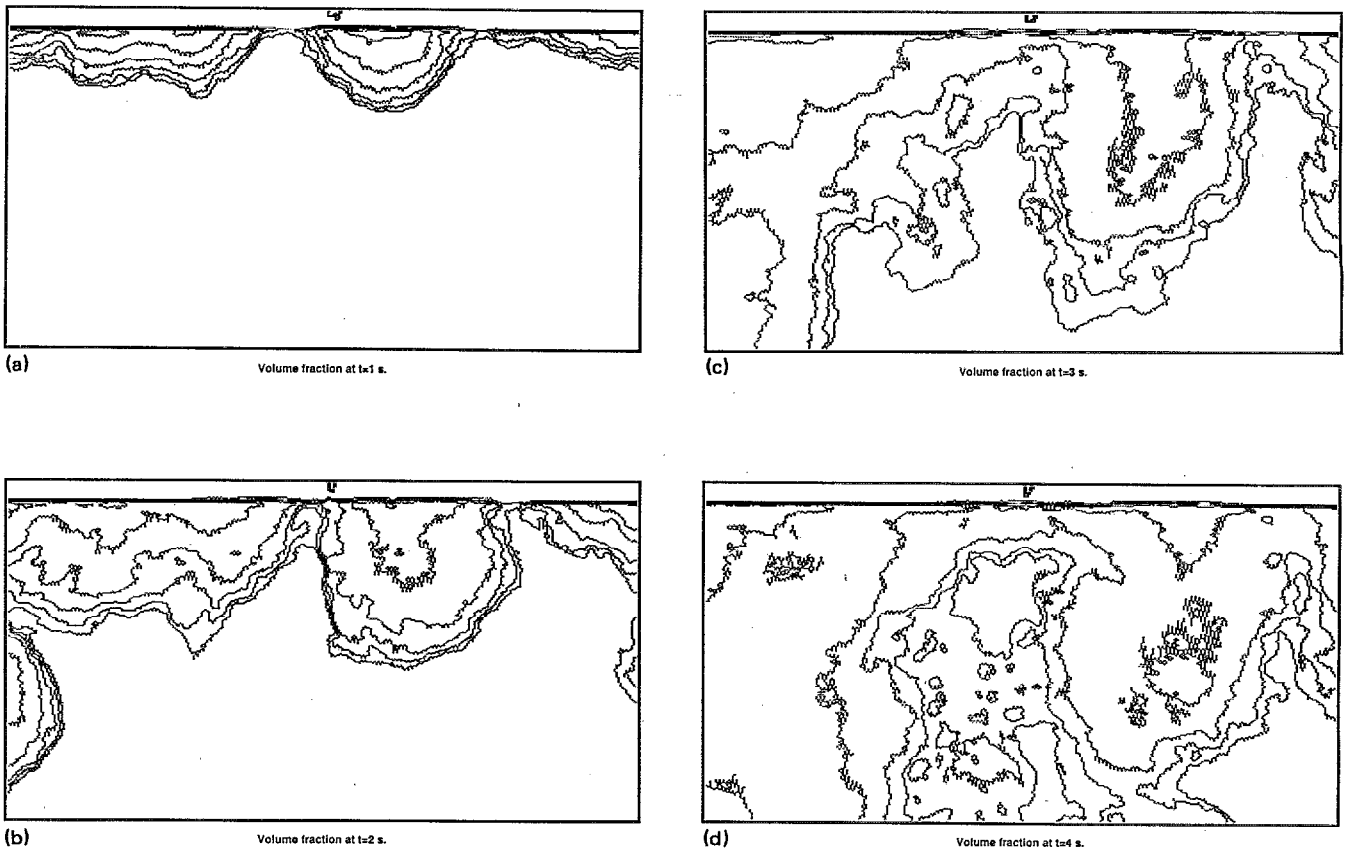

FIG. 3. Dye intensity contours measured during the advance of the mixing front for $A = 0.0015$. Each contour divides the total intensity change into five equal parts. Note the rapid change in intensity at the front of the mixing region and at the edges of the protuberances.

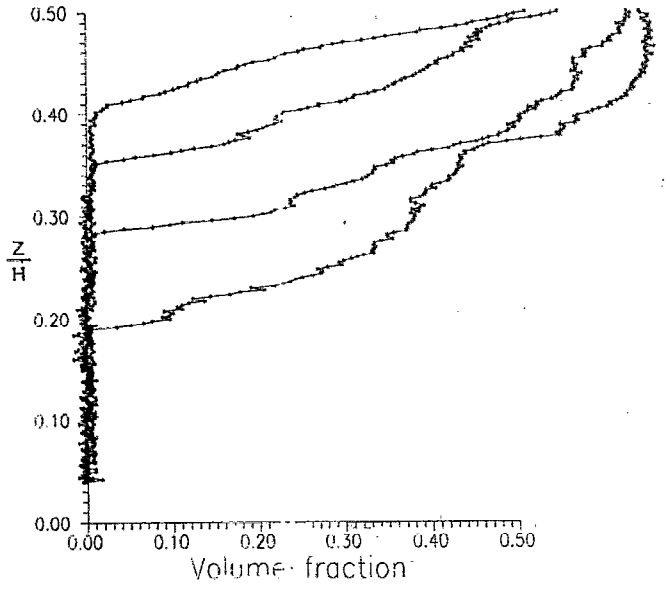

FIG. 4. Vertical profiles of horizontally averaged dye volume fraction for $A = 0.015$. The four profiles show the evolution in time of the volume fraction profile averaged over horizontal planes in the central portion of the tank.

C. Conductivity measurements

1. Single point measurements

The data collected from a single conductivity probe placed centrally 1 mm above the aluminum plate are useful for determining the behavior of the system as a function of density difference. Examples at three different initial values of $A = 0.004$, 0.012, and 0.033 are shown in Fig. 6. These plots show the normalized density $[\rho(t) - \rho_2]/(\rho_1 - \rho_2)$, where $\rho(t)$ is the density measured by the probe, so that the upper layer corresponds to 1 and the lower layer to 0, as a function of the dimensionless time. The plate is removed at $t = 0$. Since the probe is in the upper layer, the reading is 1 before the plate is removed and then decreases as lower layer fluid mixes upward.

The overall behavior is the same at all values of A, with a rapid decrease in the density being observed, followed by oscillations which eventually decay, when the probe records a density intermediate between the upper and lower values. The initial phase follows at t^2 growth consistent with (3) until $t = 2.7T$, at which point the mixing region fills the tank. Unstable stratification persists until $t \approx 10T$. After that time the density stratification is stable. All records show fine scale fluctuations superimposed on longer time scale oscillations.

Figure 7 shows the e-folding time obtained by fitting an exponential decay to the peaks of the slow time oscillations plotted against A. These peak values provide a measure of the mixing into the large-scale structures observed in the mixing region. These time scales are relatively insensitive to the values of A showing that the growth and decay of the system scales on T given by (4).

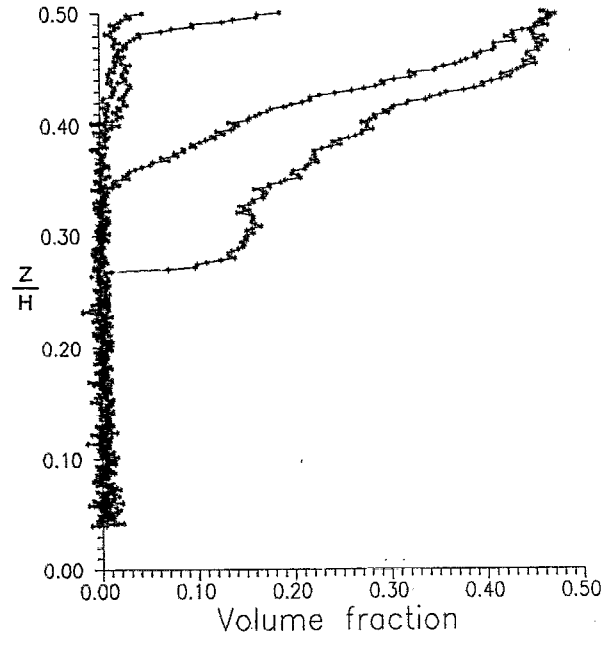

FIG. 5. Vertical profiles of dye volume fraction of the central blob of the experiment shown in Fig. 4 as it evolves in time. Note the sharpening of the front as the blob descends.

2. Multiple point measurements

Time sequences of density such as those shown in Fig. 6 were recorded by a number of probes positioned at different heights and at different horizontal positions in the upper layer. Using this data and taking ensemble averages of the results from a number of different experiments, mean values of fluctuating concentration were obtained. An estimate of the rms concentration fluctuation σ, normalized by $\rho_1 - \rho_2$, recorded at each probe was obtained by taking a running mean of the conductivity signal. Examples of the effects of different averaging times $\bar{t}$ are shown in Fig. 8. The value of $\bar{t} = 1.5$ sec was used to determine σ as this value seems to give the most reliable estimate, independent of small variations of $\bar{t}$.

Figure 9 shows σ plotted against time as measured at four positions above the plate. The arrival of the RT mixing front can be clearly seen, and then the subsequent decay in fluctuations behind the front. Note that the peak values do not change greatly with height, although there is some variation depending on whether the probe passes through the center of a descending blob or not. The maximum concentration fluctuation σ_{max} is plotted as a function of height in Fig. 10. These values are averages over five probes at each horizontal plane, and we note that there is decay in the value of σ_{max} with distance from the plate. It is also relevant to note that the values of σ_{max} are significantly less than 0.5, the value which would be obtained if there were no molecular mixing but simply an intermingling of the two fluids.

IV. MIXING EFFICIENCY

The RT experiment provides a convenient way of determining how much of the initial potential energy ($PE_{initial}$) is used to mix the fluid, and what fraction is eventually dissipated by viscosity. If no mixing occurs, as would be the case

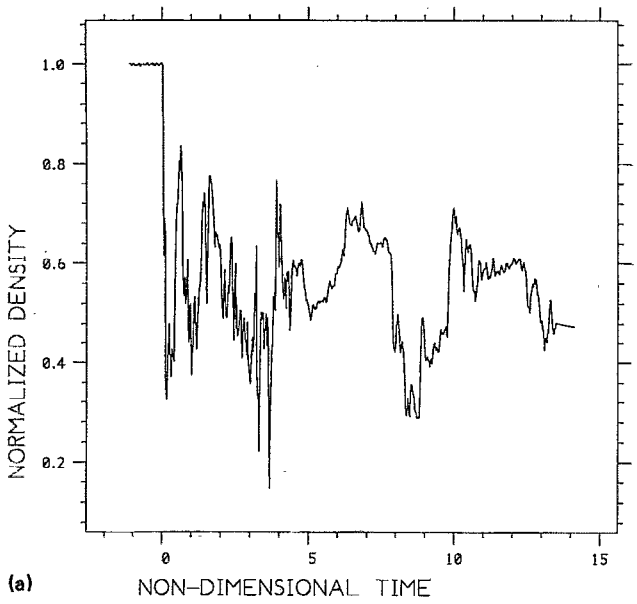

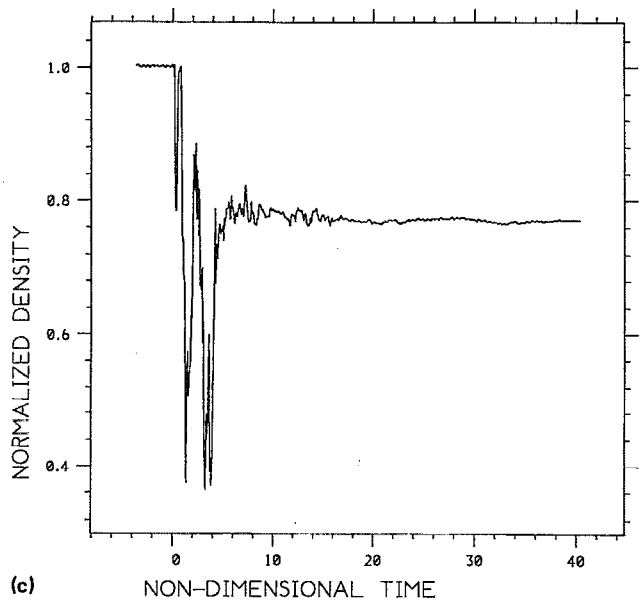

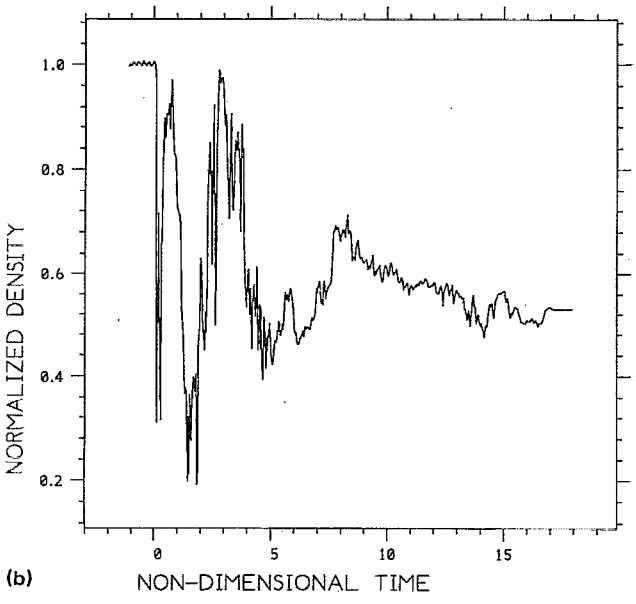

FIG. 6. Single probe density signals at the center of the tank. For experiments with different values of the Atwood number A = (a) 0.004; (b) 0.012; (c) 0.033.

with immiscible fluids, then the two layers would simply exchange places without any change in their densities.

In the experiments density profiles were measured before and after releasing the dense fluid above the lighter one. The initial profile was considered as a top-heavy step of density excess $\Delta\rho$ and the final profile was measured 4 min after the release of the dense fluid, when it was judged that most of the motion had decayed and no further change in the density profile was observed. In these experiments both upper and lower fluids had the same height, $H/2 = 200$ mm.

The potential energy decrease in the process was determined from the final density profile by calculating

$$P \equiv \mathrm{PE}_{\mathrm{final}} = g \int_0^H z\,(\rho(z)_{\mathrm{final}} - \rho_2)\,dz, \tag{7}$$

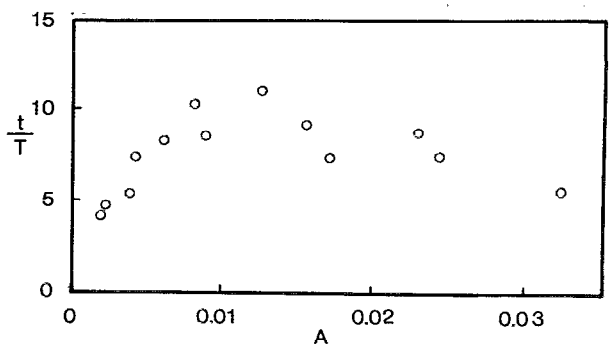

FIG. 7. The e-folding time of slow density oscillations for different initial Atwood numbers.

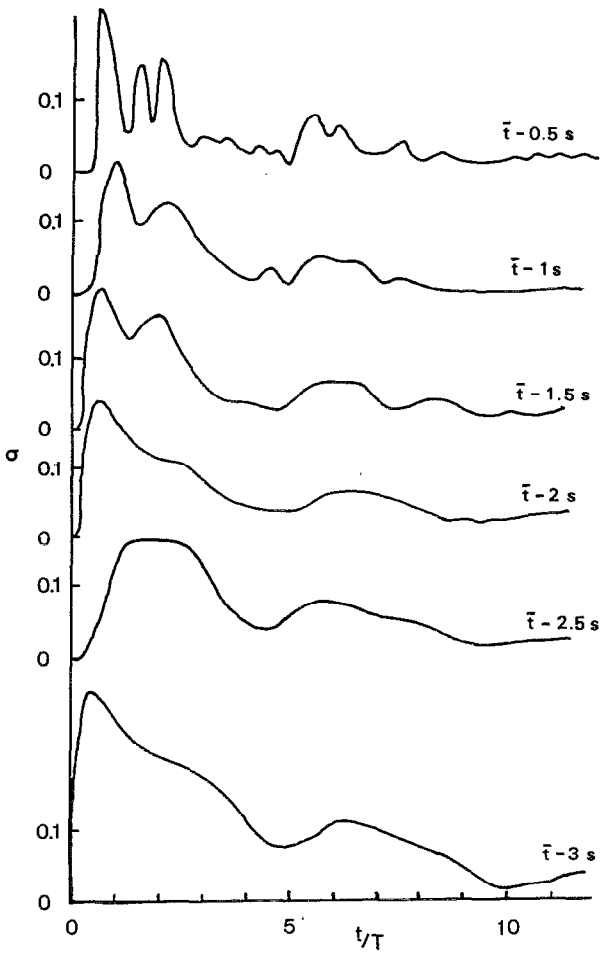

FIG. 8. Variation with time of σ the normalized rms density fluctuations for the signal 4 cm above the plate for $A = 0.010$. Different averaging times are shown in the figure, $\bar{t} = 1, 1.5, 2, 2.5, 3$ sec.

using as the initial potential energy of the top-heavy two-layer system

$$\mathrm{PE}_{\mathrm{initial}} = \tfrac{3}{4}P_0, \tag{8}$$

where

$$P_0 \equiv \tfrac{1}{8}g\Delta\rho H^2. \tag{9}$$

The calculations were done numerically, checking that mass conservation was better than 5%. In the case when there is no mixing the final potential energy is given by $P = \frac{1}{4}P_0$, while for complete mixing when the density in the tank is completely uniform, $P = \frac{1}{2}P_0$. In Fig. 11 an example of the initial and final density profiles are presented for an experiment with $A = 0.011$. Note that there is an appreciable final density gradient and that the final density at the mid-plane of the tank is close to the average density. The mixing efficiency η is defined as

$$\eta = (P - \tfrac{1}{4}P_0)/(\tfrac{3}{4}P_0 - \tfrac{1}{4}P_0). \tag{10}$$

The numerator gives the difference in potential energy between the observed final state and that in which no mixing occurs, while the denominator is the maximum amount of potential energy that can be released as the system overturns. Since complete mixing implies that $P = \frac{1}{2}P_0$, we find that

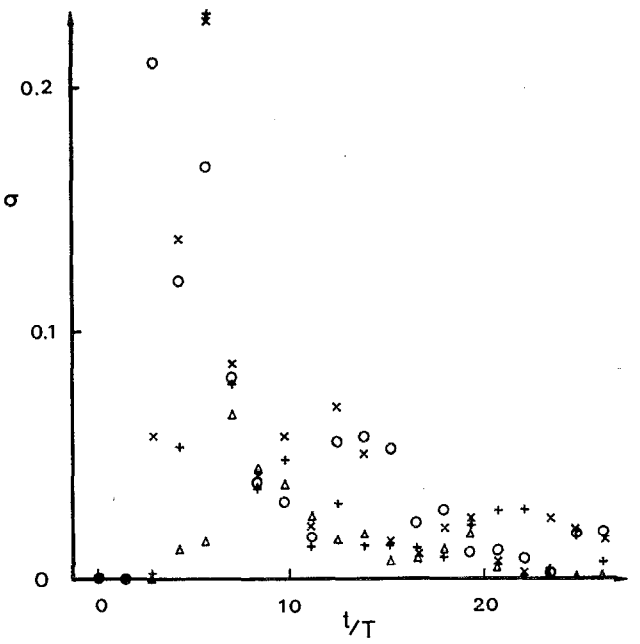

FIG. 9. Evolution of rms density fluctuations with time for each of four vertically positioned probes at 4, 6.5, 9, and 11.5 cm from the plate. The symbols indicate variations in time of the probes at different z positions: O, 4 cm; ×, 6.5 cm; +, 9 cm; △, 11.5 cm.

$0 \leqslant \eta \leqslant 0.5$. Thus in this system it is never possible to extract more than one-half of the available potential energy to do work against the stratification. This result is in contrast to other mixing studies, where, in principle at least, all of the energy appears to be available for mixing.

Values of the mixing efficiency η for the 13 experiments with initial equal dense and light fluid masses are shown in Fig. 12. Note that η increases with increasing A, and then attains a value of $\eta = 0.35$. There is perhaps a slight decrease in the mixing efficiency at the higher Atwood numbers, but

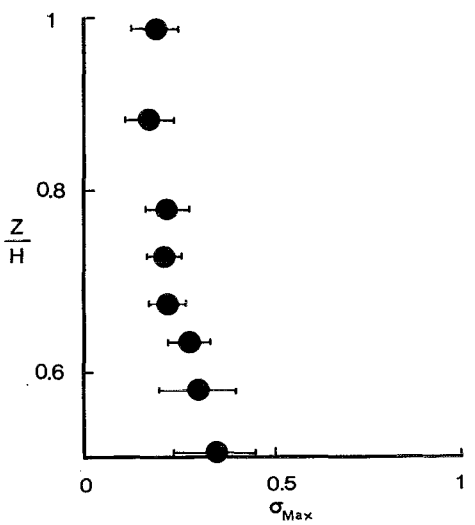

FIG. 10. Variation of the rms density fluctuations $\sigma_{\max}$ at the RT front with height for all experiments with $0.006 < A < 0.010$.

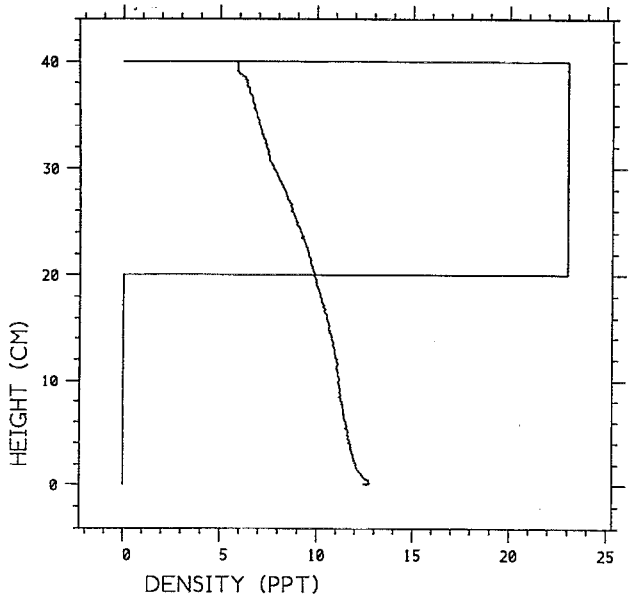

FIG. 11. The initial and final density profiles. Initially the fluid is top heavy and the final state is stably stratified.

the trend is not significant.

A surprising feature of these results is the high values of η that are obtained. In most other mixing processes the maximum values of η that have been measured are of the order of 0.2 (Linden[16,17]). The reasons for the high values attained in the RT case will be discussed in the next section.

V. DISCUSSION AND CONCLUSIONS

The advance of the RT front agrees with the work of Read[9] and Youngs,[10] who carried out experiments at much larger density ratios (Atwood numbers) than those reported here. Flow visualization has given considerable insight into the mixing processes inside the box. Presently the emerging picture of the mixing process is as follows. Initially a pure RT instability with length scale λ_m appears, together with the disturbances from the plate. The growth and merging of disturbances favors the appearance of several distinct blobs, bubbles, or protuberances which produce shear instabilities on their sides. These, in turn, sometimes develop further secondary shear instabilities. After a short period of time three-dimensional effects have broadened the spectrum of length scales, so that the full range of scales from the gravest mode comparable in size to the width of the tank to the Kolmogorov scale are present (see Redondo and Linden[18]).

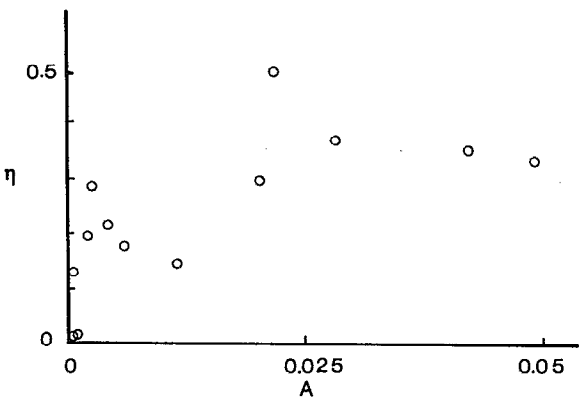

FIG. 12. Mixing efficiency versus initial Atwood numbers.

It appears that most of the mixing takes place at the sides of the large-scale protuberances, as they rise and fall into the adjacent layers. This conclusion is borne out by the flow visualization studies, and also from measurements made of the mixed product in a tracer chemical reaction that are discussed in a later paper (Redondo and Linden[13]). We also see clear evidence for it from the measurements presented here of the dye intensity profiles, which show that fluid arrives at the front of the descending protuberances with virtually no dilution (see Fig. 5). The large concentration gradients occur at the front and sides of these protuberances.

Similar conclusions can be drawn from the conductivity measurements, where it was found that the maximum rms concentration fluctuations $\sigma_{\max}$ were observed when the front of the mixing region passed the probe, and that the value of $\sigma_{\max}$ was only weakly dependent of the distance from the original interface position.

These conclusions suggest that a significant fraction of the mixing occurs before the whole system overturns, and so takes place while the fluid is *unstably* stratified. Indeed Fig. 6 suggests that once the system has overturned, there is a rapid decay in the density fluctuations. As a result higher mixing efficiencies are found in the RT experiment than is usual for mixing processes in stably stratified fluids.

It is of interest to calculate the error involved in assuming that complete mixing occurs during the RT process. This assumption is common in numerical models involving stratified fluids where it is assumed that any in any region of the fluid where isopycnals are inverted the density is readjusted to the vertical average value. This would give a mixing efficiency $\eta = 0.5$, whereas the present experiments suggest the value $\eta = 0.35$ is more accurate. Using the reduced value of η we find that after a RT mixing event such as might occur during the breaking of an internal wave, the final *stable* density gradient is approximately 11% of the original unstable gradient that initiated the instability.

ACKNOWLEDGMENTS

We would like to thank D. L. Youngs for many interesting discussions on this work, R. Perkins and S. Dalziel for their help with the digitizer, and C. Caulfield for contributing to the initial experiments.

This work has been supported by the M. O. D.

[1] Lord Rayleigh, *Scientific Papers* (Cambridge U.P., Cambridge, 1900), Vol. II, pp. 200–207.
[2] G. I. Taylor, Proc. R. Soc. London Ser. A **201**, 192 (1950).
[3] S. Chandrasekhar, *Hydrodynamic and Hydromagnetic Stability* (Oxford U.P., London, 1961).
[4] D. L. Youngs, Physica D **12**, 32 (1984).
[5] D. J. Lewis, Proc. R. Soc. London Ser. A **202**, 81 (1950).
[6] J. C. Allred and G. H. Blount, Los Alamos Scientific Laboratory Report No. LA-1600, 1954.
[7] R. E. Duff, F. H. Harlow, and C. W. Hirt, Phys. Fluids **5**, 417 (1962).
[8] H. W. Emmons, C. T. Chang, and B. C. Watson, J. Fluid Mech. **7**, 177 (1960).

[9] K. I. Read, Physica D **12**, 45 (1984).
[10] D. L. Youngs, Physica D **37**, 270 (1989).
[11] P. F. Linden, J. M. Redondo, and C.-C. P. Caulfield, in *Proceedings of the Workshop on the Physics of Compressible Turbulent Mixing*, edited by A. C. Buckingham (Princeton U.P., Princeton, NJ, 1988).
[12] J. M. Redondo, Thesis Doctoral, Universidad de Barcelona, 1987.
[13] J. M. Redondo and P. F. Linden, submitted to J. Fluid Mech.
[14] J. M. Redondo and P. F. Linden, in *Proceedings of the 3rd IMA Conference on Stably Stratified Flows*, edited by S. D. Mobbs and J. C. King (Oxford U.P., London, 1991).
[15] H. J. Pearson and P. F. Linden, J. Fluid Mech. **134**, 195 (1983).
[16] P. F. Linden, Geophys. Astrophys. Fluid Dyn: **13**, 3 (1979).
[17] P. F. Linden, J. Fluid Mech. **100**, 691 (1980).
[18] J. M. Redondo and P. F. Linden, in *Proceedings of the IMA Conference on Mathematics and Computations of Deforming Surfaces*, edited by J. C. R. Hunt, D. G. Dritschel, and R. Perkins (Oxford U.P., London, 1990).